

## Supplementary Information

### Pressure-induced superelastic behaviour of isonicotinamide

Eleanor C.L. Jones,<sup>a\*</sup> Suse S. Bebiano,<sup>a,b</sup> Martin R. Ward,<sup>a</sup> Luis M. Bimbo<sup>a,c,d</sup> and Iain D.H. Oswald<sup>a\*</sup>

<sup>a</sup>Strathclyde Institute of Pharmacy & Biomedical Sciences (SIPBS), University of Strathclyde, 161 Cathedral Street, G4 0RE, Glasgow, U.K. email: eleanor.jones@strath.ac.uk; iain.oswald@strath.ac.uk

<sup>b</sup>EPSRC Centre for Innovative Manufacturing in Continuous Manufacturing and Crystallisation, University of Strathclyde, Technology Innovation Centre, 99 George Street, Glasgow, G1 1RD, U.K.

<sup>c</sup>Department of Pharmaceutical Technology, Faculty of Pharmacy, University of Coimbra, Coimbra, Portugal.

<sup>d</sup> CNC - Center for Neuroscience and Cell Biology, and CIBB - Center for Innovative Biomedicine and Biotechnology, Rua Larga, University of Coimbra, 3004-504 Coimbra, Portugal.

## Experimental Section

### Crystal formation

Form I was recrystallised from a solution of isonicotinamide (Sigma Aldrich, 99% purity) in ethanol (80 mg/mL, Fisher Scientific, 99.8% purity) at 22 °C. The solution was stirred for 60 minutes and filtered into a clean vial using PTFE syringe filter (0.2 µm). Colourless block crystals were produced by slow evaporation of the solvent and characterised using X-ray diffraction and Raman spectroscopy before loading into a diamond anvil cell.

### Diamond anvil cell

Merrill-Bassett diamond anvil cells (DAC) were used to apply pressure to single crystals of isonicotinamide during the X-ray and Raman studies. A pre-indented tungsten foil gasket (99.95 %, Hollinbrow, Telford, UK) was placed between two diamonds with 600 µm culets. The gasket, 250 µm in thickness, was pre-indented to approximately 100 µm before a 250 µm hole was drilled through the foil to serve as a sample chamber. Petroleum ether (PET 35/60, Alfa Aesar) was used as the hydrostatic medium.<sup>1</sup> The pressure of the cell was monitored using fluorescent R-line of crushed ruby spheres within the chamber of the cell, compared to those at ambient pressure.<sup>2</sup>

### Single-crystal X-ray diffraction (SC-XRD)

Single crystal X-ray diffraction data were collected for ambient crystals using a Bruker D8 Venture diffractometer with a Photon II pixel array detector and Incoatec IµS microfocus Cu X-ray source ( $K\alpha_1$   $\lambda = 1.54178$  Å). Data were reduced using SAINT within the APEX3 suite of software.<sup>3,4</sup> SADABS was used to correct for absorption.<sup>5</sup> OLEX2 v1.2 software was used to refine the structures, with coordinates taken from EHOWIH01 (Cambridge Structural Database, CSD).<sup>6-8</sup>

High pressure diffraction data was collected using Bruker APEX-II diffractometer with Incoatec IµS microfocus Mo X-ray source ( $K\alpha_1$   $\lambda = 0.71073$  Å) and CCD detector. Data were reduced using SAINT within APEX3 using the dynamic masking procedures.<sup>3,4</sup> SADABS was used for absorption correction.<sup>5</sup> The structures were refined in OLEX2 v1.2.<sup>6</sup>

Refinement against the pressure data were conducted using the coordinates of the ambient form, collected from the CSD (ref code: EHOWIH01).<sup>7,8</sup> The refined atomic coordinates at each pressure were used as the input for each subsequent data set. Non-hydrogen atoms were treated using anisotropic displacement parameters. RIGU restraints were applied to all non-hydrogen atoms. 10 data sets were collected between 1.58 and 5.65 GPa for Form I using two different crystals. Crystal 1 was collected at 1.90, 2.40, 3.23, 4.00 and 5.65 GPa. Crystal 2 was collected at 1.58, 3.46, 3.99, 4.33 and 4.98 GPa.

## Raman spectroscopy

Raman spectra were collected using a Horiba Scientific Raman XploRA™ PLUS microscope with a 532 nm laser source. Acquisition parameters including accumulation, acquisition time, grating, slit and hole were varied to maximise the signal for each data collection. Raman spectra were taken in the region of 50 to 3500  $\text{cm}^{-1}$ . The diamond peak at 1300-1350  $\text{cm}^{-1}$  is omitted for clarity.

## Periodic DFT calculations

Geometry optimisations of isonicotinamide were performed by periodic Density Functional Theory (DFT) using the DMOL3 code<sup>9</sup> found in Materials Studio.<sup>10</sup> The DNP numerical basis set<sup>9</sup> was used together with the PBE functional<sup>11</sup> with dispersion correction applied (Tkatchenko- Scheffler).<sup>12</sup> The models from the single crystal refinements were used and the unit cell dimensions were fixed at the values obtained from the experimental data and the atomic coordinates were allowed to optimise. Convergence was defined when the maximum changes in total energy, displacement and gradient were  $10^{-5}$  Ha,  $5 \times 10^{-3}$  Å and  $2 \times 10^{-3}$  Ha Å<sup>-1</sup>, respectively. Brillouin zone integrations were performed by Monkhorst-Pack<sup>13</sup>  $k$ -point sampling at intervals of 0.07 Å<sup>-1</sup>.

## PIXEL calculations

PIXEL calculations were performed on each dataset from ambient to 5.65 GPa using the MrPIXEL program.<sup>14</sup> Molecular electron densities were calculated using Gaussian09W at the B3LYP/6-31G\*\* level.<sup>15</sup> The condensation level was set to 4 and cluster radius was 14 Å. The most energetic intermolecular interactions of Form I and Form I' are displayed in Table S5 and relationship between molecular pairs visualised using Mercury (Fig. S7).<sup>16</sup>

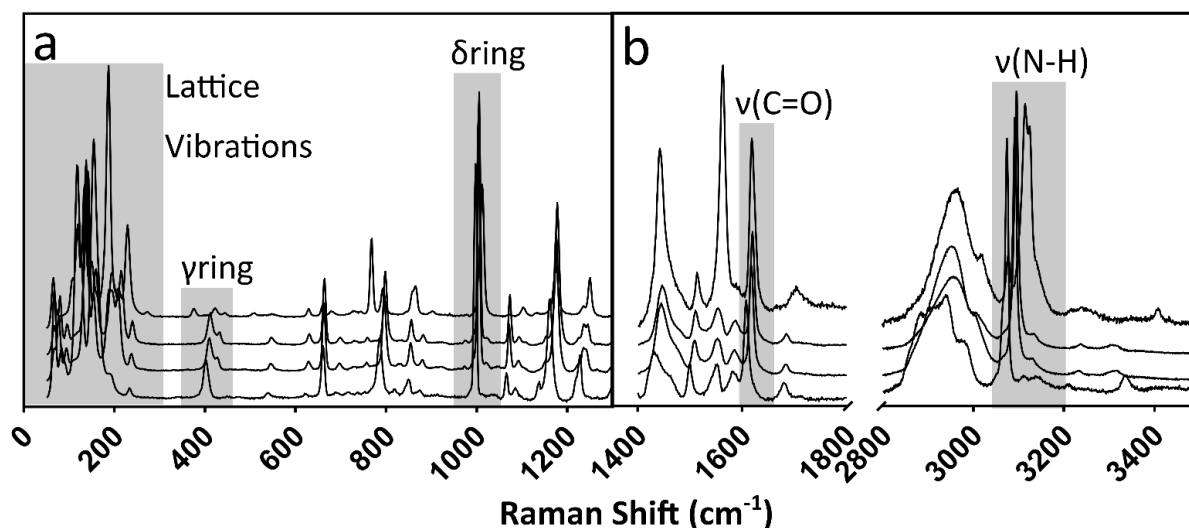


**Fig. S1.** Raman spectra of Form I isonicotinamide at various pressures during compression a) 50-1300  $\text{cm}^{-1}$  and b) 1400-3500  $\text{cm}^{-1}$ . Pressure increases from bottom to top: 1.58, 3.99, 4.33 and 4.98 GPa. The diamond peak at 1300  $\text{cm}^{-1}$  and between 1800-2800  $\text{cm}^{-1}$  were excluded.  $\gamma$ , out-of-plane bending;  $\delta$ , in-plane bending;  $\nu$ , stretching

The initial Raman spectra indicates that the environment of the pyridine ring is altered as the crystal changes. The out-of-plane (oop) bending ( $400 \text{ cm}^{-1}$ )<sup>17,18</sup> and in-plane bending (ip; 660, 663 and 664  $\text{cm}^{-1}$ ) show distinct changes where the oop bend splits into two peaks with an additional band at 374  $\text{cm}^{-1}$  appearing. The ip bends all soften to lower frequencies which is indicative of a potential phase transition (Fig.S1a and b). Further evidence of the change is observed around the N-H stretch (3072  $\text{cm}^{-1}$ ) where it splits into three separate peaks (3075, 3113 and 3127  $\text{cm}^{-1}$ ). From the discontinuities in the Raman behaviour, it suggests that the phase transition between 4.33 and 4.98 GPa alters the environment of the pyridine ring system.

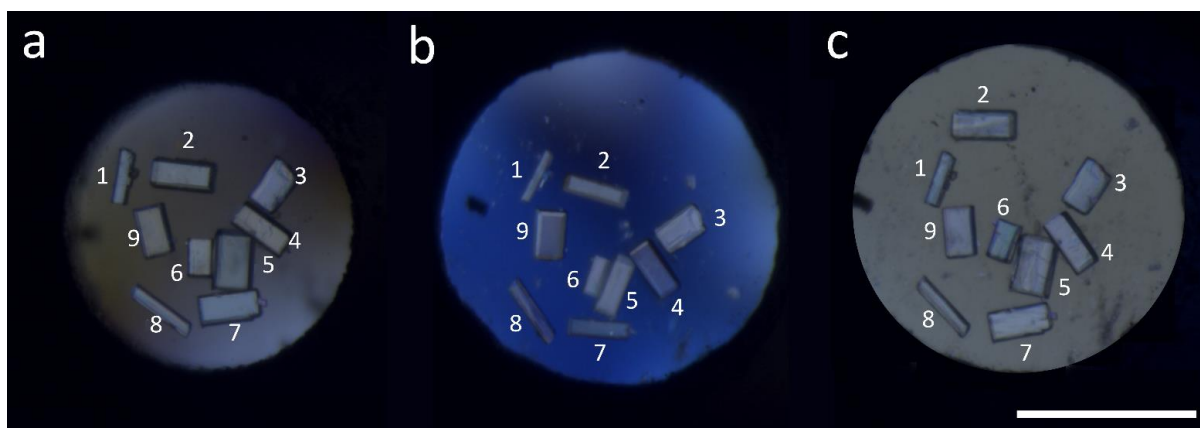


**Fig. S2.** Microscopy image of isonicotinamide Form I loaded in a gas membrane cell at a) ambient pressure and b) after the phase transition 5.29 GPa showing changes to crystal dimensions. c) shows the crystals back at ambient, with restoration back to their original dimensions. Scale bar represents 200  $\mu\text{m}$ .

**Table S1.** Crystal dimensions and aspect ratios of Form I isonicotinamide crystals during compression to 5.29 GPa and decompression.

Crystal No.	Dimensions ( $\mu\text{m}$ )		Aspect Ratio		Dimensions ( $\mu\text{m}$ )		Aspect Ratio
	Ambient	5.29 GPa	Ambient	5.29 GPa	Ambient (after decompression)		
1	16.8	11.7	3.5	5.4	19	3.1	
	59	63.1			59		
2	30.9	19.8	2.1	3.4	32.3	2.1	
	64.2	68.3			68.1		
3	32	33	1.6	1.6	36.1	1.6	
	51.6	51.3			56.6		
4	24.8	28.2	2.5	2.2	28.9	2.3	
	63.2	61.3			65.3		
5	39.8	24.7	1.7	2.5	39.6	1.6	
	67.2	62.4			64		
6	27.6	12.2	1.5	3.3	27.4	1.5	
	41.8	40.5			42		
7	33.2	17	2.0	3.9	33.7	1.9	

	67.8	66.7			62.9	
<b>8</b>	15	17.6	5.2	4.2	15.4	5.0
	77.4	73.5			77	
<b>9</b>	32.1	31.5	1.7	1.7	34	1.7
	54.6	54.4			58.2	

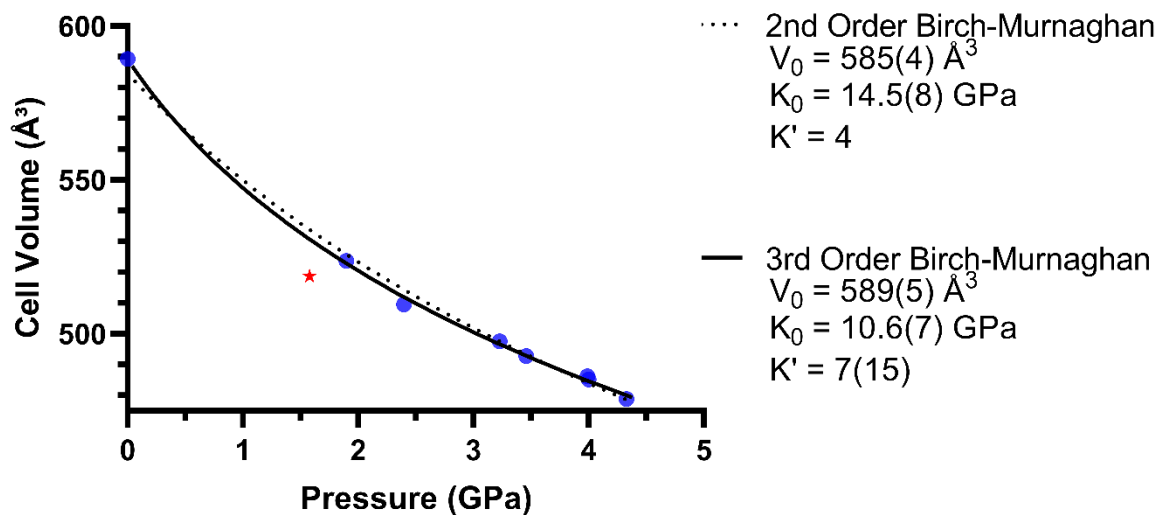


**Fig. S3.** 2<sup>nd</sup> and 3<sup>rd</sup> Order Birch-Murnaghan Equation of State for Form I isonicotinamide from ambient pressure to 4.33 GPa (before transition). Data point at 1.58 GPa was not used in the calculation due to poor fit (red star). 3<sup>rd</sup> order Birch-Murnaghan displays a slightly improved fit.

**Table S2.** Crystallographic data for the compression study of Form I isonicotinamide from ambient to 3.46 GPa. The pressure points in bold are from crystal number 2.

	ISO1_01	ISO1_02	ISO1_03	ISO1_04	ISO1_05	ISO1_06
Pressure/ GPa	Ambient	<b>1.58</b>	1.90	2.40	3.23	<b>3.46</b>
<i>a, b, c</i> (Å)	10.229 (3), 5.7538 (16), 10.095 (3)	9.599 (2), 5.6979 (4), 9.7492 (7)	9.629 (2), 5.7123 (7), 9.773 (2)	9.528 (5), 5.6786 (15), 9.709 (6)	9.4148 (10), 5.6817 (4), 9.6396 (12)	9.3656 (17), 5.6791 (3), 9.6213 (6)
$\beta$ (°)	97.277 (18)	103.402 (14)	103.03 (2)	104.08 (5)	105.208 (11)	105.642 (11)
<i>V</i> (Å <sup>3</sup> )	589.3 (3)	518.68 (12)	523.70 (18)	509.5 (4)	497.58 (9)	492.79 (10)
$\mu$ (mm <sup>-1</sup> )	0.81	0.11	0.11	0.11	0.12	0.12
Crystal size (mm)	0.1 × 0.1 × 0.1	0.08 × 0.06 × 0.03	0.17 × 0.11 × 0.05	0.17 × 0.11 × 0.05	0.17 × 0.11 × 0.05	0.08 × 0.06 × 0.03
Diffractometer	Bruker APEX-II CCD					
Absorption correction	Multi-scan SADABS2016/2 (Bruker,2016/2) was used for absorption correction. wR2(int) was 0.0997 before and 0.0633 after correction. The Ratio of minimum to maximum transmission is 0.7213. The $\lambda/2$ correction factor is Not present.	Multi-scan SADABS2016/2 (Bruker,2016/2) was used for absorption correction. wR2(int) was 0.0877 before and 0.0499 after correction. The Ratio of minimum to maximum transmission is 0.9021. The $\lambda/2$ correction factor is Not present.	Multi-scan SADABS2016/2 (Bruker,2016/2) was used for absorption correction. wR2(int) was 0.1065 before and 0.0474 after correction. The Ratio of minimum to maximum transmission is 0.8927. The $\lambda/2$ correction factor is Not present.	Multi-scan SADABS2016/2 (Bruker,2016/2) was used for absorption correction. wR2(int) was 0.0761 before and 0.0452 after correction. The Ratio of minimum to maximum transmission is 0.8725. The $\lambda/2$ correction factor is Not present.	Multi-scan SADABS2016/2 (Bruker,2016/2) was used for absorption correction. wR2(int) was 0.0703 before and 0.0431 after correction. The Ratio of minimum to maximum transmission is 0.9092. The $\lambda/2$ correction factor is Not present.	Multi-scan SADABS2016/2 (Bruker,2016/2) was used for absorption correction. wR2(int) was 0.0860 before and 0.0474 after correction. The Ratio of minimum to maximum transmission is 0.8990. The $\lambda/2$ correction factor is Not present.
<i>T</i> <sub>min</sub> , <i>T</i> <sub>max</sub>	0.543, 0.753	0.640, 0.745	0.665, 0.745	0.650, 0.745	0.677, 0.745	0.670, 0.745
No. of measured, independent and observed [ <i>I</i> > 2 $\sigma$ ( <i>I</i> )] reflections	4398, 1075, 823	2303, 281, 233	2034, 285, 255	999, 259, 233	2101, 270, 249	2165, 271, 211
<i>R</i> <sub>int</sub>	0.049	0.049	0.030	0.027	0.029	0.061
$\theta$ <sub>max</sub> (°)	68.4	23.3	23.2	23.3	23.3	23.3
(sin $\theta/\lambda$ ) <sub>max</sub> (Å <sup>-1</sup> )	0.603	0.556	0.555	0.556	0.556	0.556
<i>R</i> [ <i>F</i> <sup>2</sup> > 2 $\sigma$ ( <i>F</i> <sup>2</sup> )], <i>wR</i> ( <i>F</i> <sup>2</sup> ), <i>S</i>	0.042, 0.109, 1.07	0.035, 0.085, 1.18	0.038, 0.109, 1.08	0.039, 0.110, 1.17	0.036, 0.100, 1.20	0.040, 0.109, 1.08
No. of reflections	1075	281	285	259	270	271
No. of parameters	83	106	83	82	82	82
No. of restraints	0	61	60	60	60	60
H-atom treatment	H-atom parameters constrained	All H-atom parameters refined	H-atom parameters constrained	H-atom parameters constrained	H-atom parameters constrained	All H-atom parameters refined
$\Delta\rho$ <sub>max</sub> , $\Delta\rho$ <sub>min</sub> (e Å <sup>-3</sup> )	0.15, -0.20	0.10, -0.10	0.12, -0.13	0.08, -0.11	0.09, -0.12	0.12, -0.13

**Table S3.** Crystallographic data from 3.99 to 5.65 GPa.

	ISO1_07	ISO1_08	ISO1_09	ISO1_10	ISO1_11
Pressure (GPa)	3.99	4.00	4.33	4.98	5.65
$a, b, c$ (Å)	9.300 (3), 5.6768 (6), 9.5955 (11)	9.2976 (12), 5.6740 (4), 9.5819 (15)	9.2314 (19), 5.6679 (4), 9.5601 (6)	13.149 (8), 3.4103 (10), 10.173 (2)	13.177 (9), 3.4083 (19), 10.184 (9)
$\beta$ (°)	106.32 (2)	106.290 (13)	106.813 (12)	93.11 (4)	93.15 (7)
$V$ (Å <sup>3</sup> )	486.19 (19)	485.19 (11)	478.83 (11)	455.5 (3)	456.7 (6)
$\mu$ (mm <sup>-1</sup> )	0.12	0.12	0.12	0.13	0.13
Crystal size (mm)	0.08 × 0.06 × 0.03	0.17 × 0.11 × 0.05	0.08 × 0.06 × 0.03	0.06 × 0.03 × 0.02	0.16 × 0.08 × 0.05
Diffractometer	Bruker APEX- II CCD				
Absorption correction	Multi-scan SADABS2016/ 2 (Bruker,2016/ 2) was used for absorption correction. wR2(int) was 0.0982 before and 0.0541 after correction. The Ratio of minimum to maximum transmission is 0.8104. The $\lambda/2$ correction factor is Not present.	Multi-scan SADABS2016/ 2 (Bruker,2016/ 2) was used for absorption correction. wR2(int) was 0.0978 before and 0.0437 after correction. The Ratio of minimum to maximum transmission is 0.8753. The $\lambda/2$ correction factor is Not present.	Multi-scan SADABS2016/ 2 (Bruker,2016/ 2) was used for absorption correction. wR2(int) was 0.0734 before and 0.0457 after correction. The Ratio of minimum to maximum transmission is 0.9046. The $\lambda/2$ correction factor is Not present.	Multi-scan SADABS2016/ 2 (Bruker,2016/ 2) was used for absorption correction. wR2(int) was 0.0927 before and 0.0387 after correction. The Ratio of minimum to maximum transmission is 0.8068. The $\lambda/2$ correction factor is Not present.	Multi-scan SADABS2016/ 2 (Bruker,2016/ 2) was used for absorption correction. wR2(int) was 0.1035 before and 0.0347 after correction. The Ratio of minimum to maximum transmission is 0.6859. The $\lambda/2$ correction factor is Not present.
$T_{\min}, T_{\max}$	0.604, 0.745	0.652, 0.745	0.674, 0.745	0.601, 0.745	0.511, 0.745
No. of measured, independent and observed [ $I > 2\sigma(I)$ ] reflections	2132, 261, 192	2056, 265, 237	2103, 256, 205	945, 234, 155	591, 238, 119
$R_{\text{int}}$	0.078	0.031	0.054	0.054	0.061
$\theta_{\text{max}}$ (°)	23.3	23.3	23.2	22.9	23.3
$(\sin \theta/\lambda)_{\text{max}}$ (Å <sup>-1</sup> )	0.556	0.556	0.554	0.548	0.555
$R[F^2 > 2\sigma(F^2)], wR(F^2),$ $S$	0.047, 0.126, 1.09	0.035, 0.094, 1.14	0.039, 0.098, 1.15	0.050, 0.131, 1.20	0.045, 0.135, 1.00
No. of reflections	261	265	256	234	238
No. of parameters	82	82	82	82	82
No. of restraints	60	60	60	135	62
H-atom treatment	H-atom parameters constrained	H-atom parameters constrained	H-atom parameters constrained	H-atom parameters constrained	H-atom parameters constrained
$\Delta\rho_{\text{max}}, \Delta\rho_{\text{min}}$ (e Å <sup>-3</sup> )	0.14, -0.15	0.09, -0.14	0.11, -0.13	0.13, -0.13	0.12, -0.14

Computer programs: SAINT V8.38A<sup>3</sup>, SHELXT<sup>19</sup>, XL<sup>20</sup>

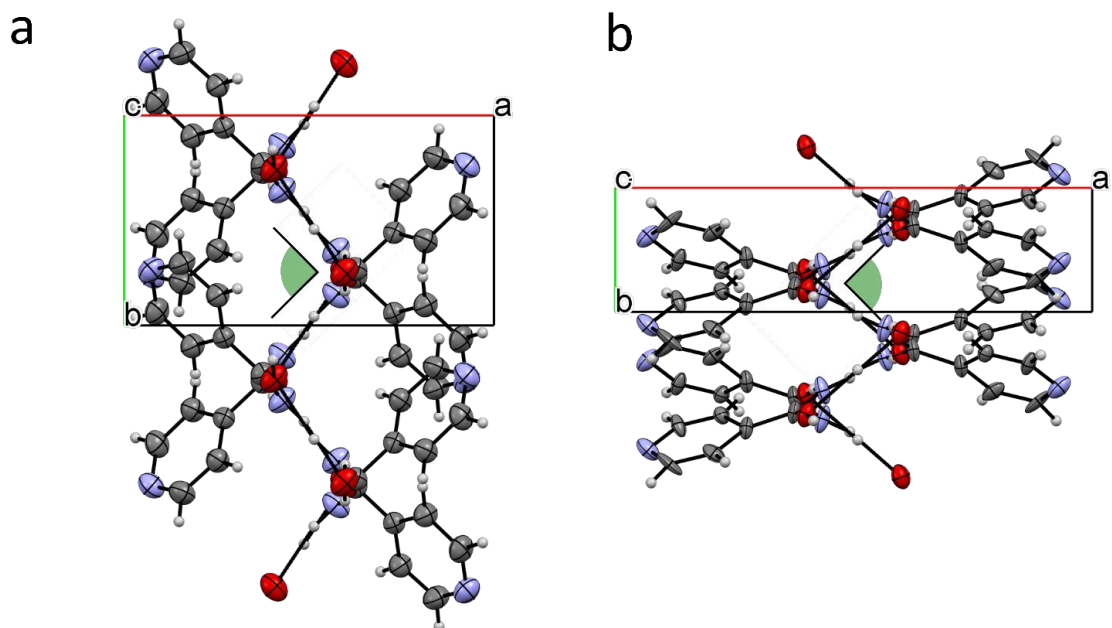


**Fig. S4.** Crystal structures of isonicotinamide Form I and Form I' are shown in figures a) and b) respectively. The structures are shown looking down the crystallographic *c*-axis. Neighbouring dimers are rotated by  $57.80^\circ$  at 4.33 GPa and  $59.16^\circ$  after the transition.

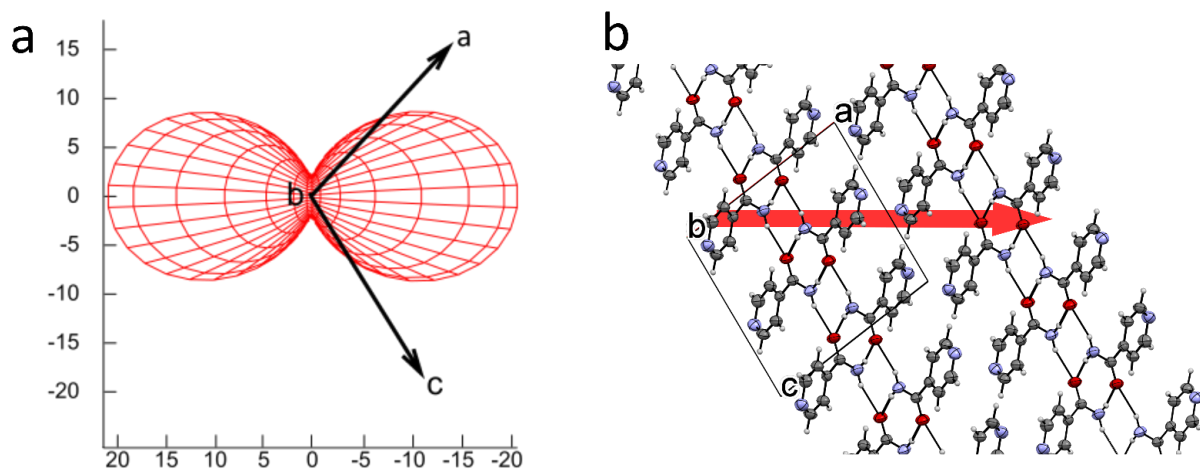


**Fig. S5.** a) Compressibility of Form I isonicotinamide as calculated by PASCAL.<sup>21</sup> b) Compression occurs between the *a*- and *c*-axis.

**Table S4.** Total lattice energy of Form I isonicotinamide as calculated by Pixel using the MrPIXEL routine for file set-up.<sup>14,16</sup> Each structure was geometry optimised prior to PIXEL calculations to account for any errors in the models derived from the low completeness of the high-pressure datasets.

Pressure (GPa)	Coulombic (kJ mol <sup>-1</sup> )	Polarisation (kJ mol <sup>-1</sup> )	Dispersion (kJ mol <sup>-1</sup> )	Repulsion (kJ mol <sup>-1</sup> )	Total (kJ mol <sup>-1</sup> )
0.0001	-94.4	-33.9	-89.1	103.7	-113.6
1.58	-127.7	-50.2	-122.5	188.7	-111.8
1.9	-122.9	-48.7	-120	179.4	-112.2
2.4	-134	-53.5	-128	206.2	-109.4
3.23	-143.6	-59.2	-136	230.1	-108.6
3.46	-146.9	-61.1	-139.3	240.8	-106.5
3.99	-152.2	-63.4	-144.1	255.6	-104.1
4.0	-153.8	-64.1	-144.9	258.9	-103.9
4.33	-159.2	-66.5	-149.8	276	-99.5
4.98	-153.6	-68.5	-168	304.4	-85.8
5.65	-152	-68.4	-166.5	300	-86.8

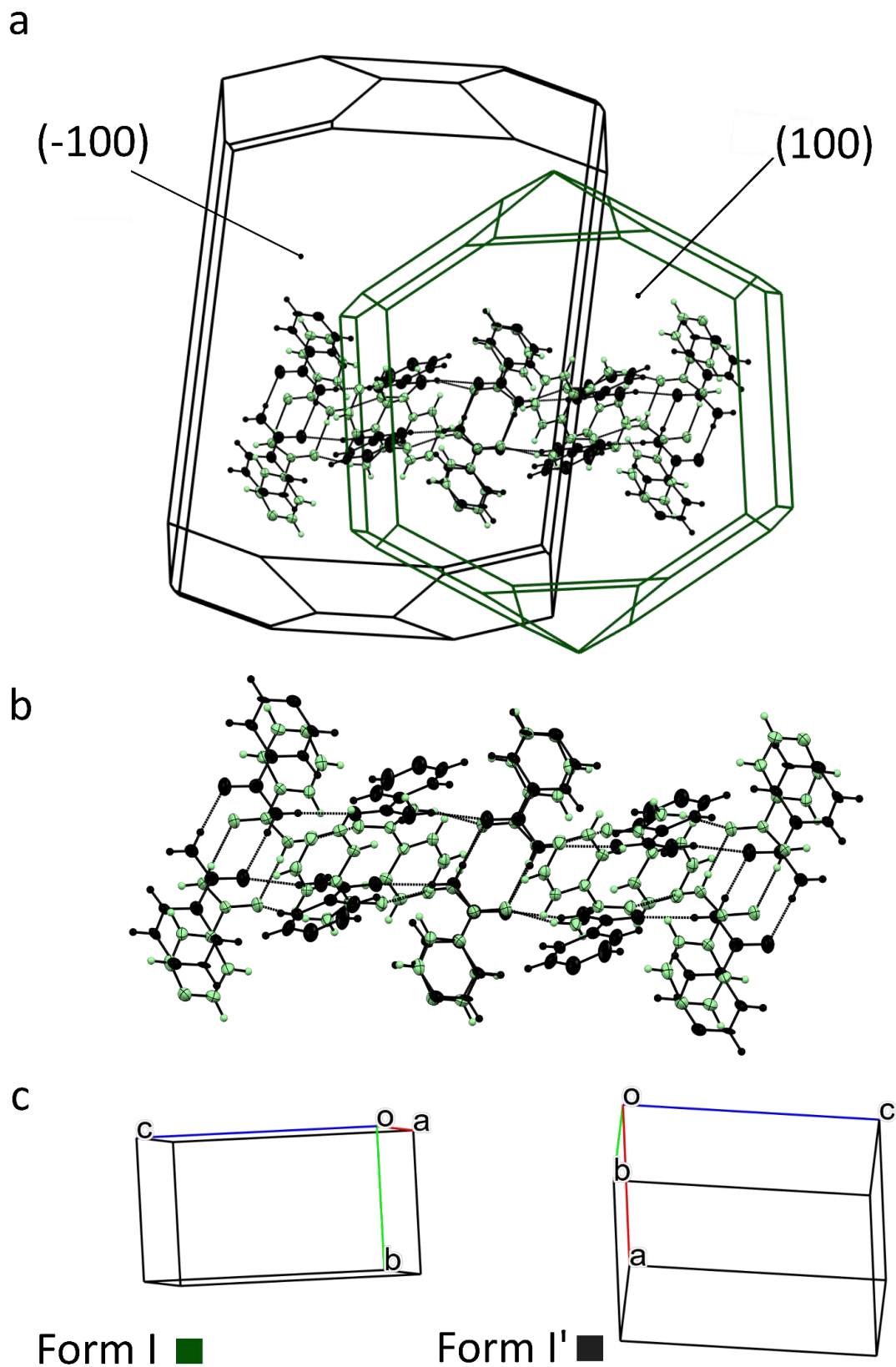


**Fig. S6.** a) Bravais, Friedel, Donnay and Harker (BFDH) model of the crystal morphology of Form I isonicotinamide at 4.33 GPa (green) and Form I' at 4.98 GPa (black), with b) crystal structures overlaid to show rotation of the molecules after the transition. c) Unit cell of isonicotinamide before and after the transition to indicate the relative orientation.

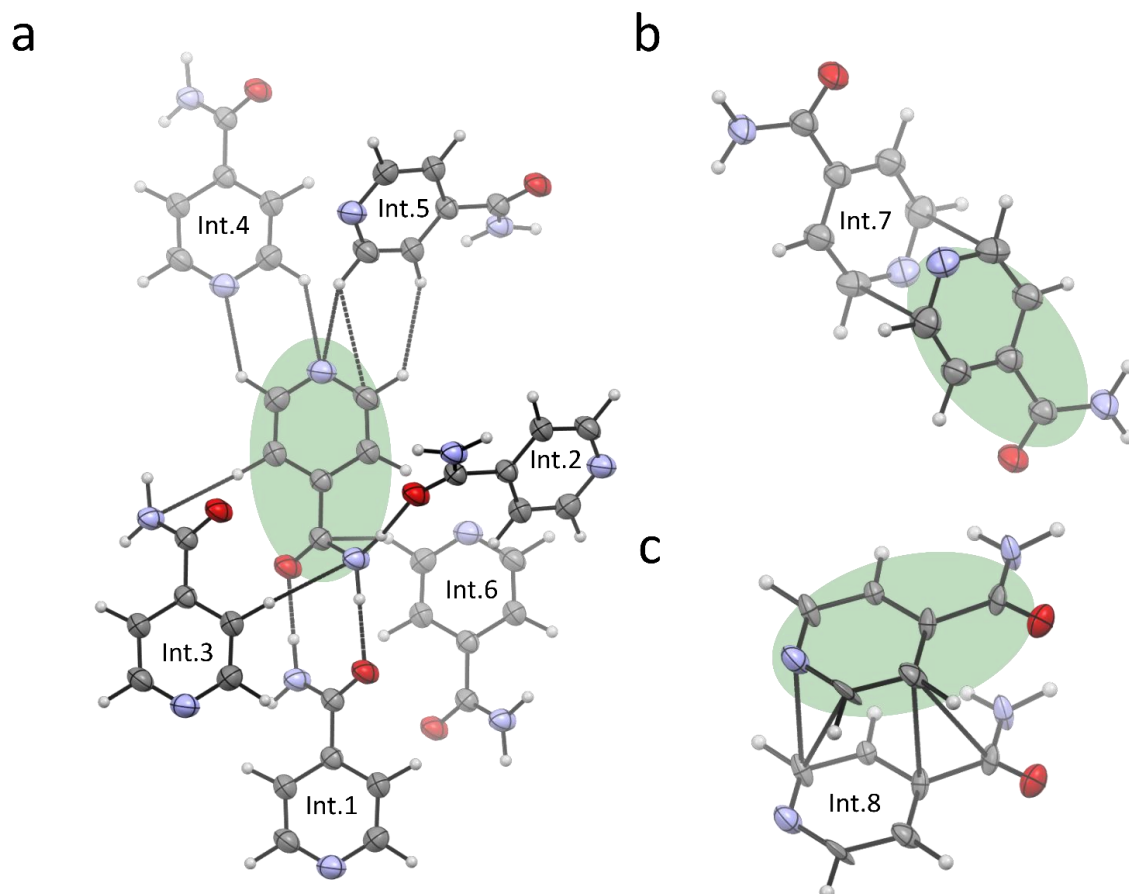


**Fig. S7.** Highest energy interactions of a) Form I and Form I' isonicotinamide, b) Form I only and c) Form I' only as calculated by Pixel using the MrPIXEL routine in Mercury API module.<sup>14,16</sup> The central molecule is highlighted in green. Depth cue is used to show difference in layers between central and interacting molecule.

**Table S5.** Intermolecular interactions during the compression of Form I isonicotinamide, as calculated by Pixel using the MrPIXEL routine for file set-up.<sup>14,16</sup> Each structure was geometry optimised before the PIXEL calculations to account for any errors in the models derived from the low completeness of the high-pressure datasets. Eight significant interactions have been chosen. Energies for Form I' are highlighted in grey.

Pressure (GPa)	Centroid distance (Å)	Coloumbic (kJ mol <sup>-1</sup> )	Polarisation (kJ mol <sup>-1</sup> )	Dispersion (kJ mol <sup>-1</sup> )	Repulsion (kJ mol <sup>-1</sup> )	Total Energy (kJ mol <sup>-1</sup> )
Interaction 1 (Form I and Form I')						
0	7.553	-88.1	-29.2	-19.1	74	-62.4
1.58	7.44	-103.9	-37.2	-21	99.8	-62.3
1.9	7.451	-100.7	-36.4	-20.5	96.4	-61.2
2.4	7.417	-108.2	-39.3	-21.6	107	-62.1

3.23	7.403	-111.1	-40.4	-22	111.1	-62.4
3.46	7.395	-111.8	-40.8	-22.1	113.3	-61.3
3.99	7.387	-112.5	-41.1	-22.3	115.6	-60.3
4	7.385	-113.4	-41.5	-22.3	116.7	-60.6
4.33	7.372	-114	-42.2	-22.7	120.7	-58.1
4.98	7.395	-97.9	-35.4	-21.3	96.3	-58.4
5.65	7.406	-97.6	-36.7	-20.6	93.7	-61.2
Interaction 2 (Form I and Form I')						
0	5.598	-34.3	-12.1	-14	27.1	-33.2
1.58	5.481	-44.1	-18	-18.1	48.6	-31.5
1.9	5.491	-43	-17.3	-17.8	46.8	-31.3
2.4	5.465	-45.4	-18.8	-18.7	51.8	-31.2
3.23	5.444	-48.4	-20.9	-19.3	58.2	-30.5
3.46	5.437	-49	-21.4	-19.6	59.9	-30.1
3.99	5.433	-50.5	-22.2	-20	63.2	-29.6
4	5.427	-51.2	-22.6	-20.1	64.4	-29.6
4.33	5.422	-52.3	-23.1	-20.5	67.5	-28.3
4.98	5.223	-46.7	-19.9	-30	64.3	-32.3
5.65	5.228	-45.7	-19.7	-30	63.7	-31.8
Interaction 3 (Form I and Form I')						
0	5.403	-3	-2.5	-13.8	5.6	-13.7
1.58	5.177	-7.3	-5.9	-21.4	19	-15.7
1.9	5.186	-6.7	-5.6	-21.1	17.7	-15.7
2.4	5.149	-8.4	-6.7	-22.6	22.1	-15.6
3.23	5.104	-10.2	-7.8	-24.5	27.4	-15.1
3.46	5.092	-10.6	-8	-25.1	29.2	-14.6
3.99	5.062	-11.6	-8.7	-26.3	33.1	-13.6
4	5.059	-11.7	-8.8	-26.4	33.4	-13.6

4.33	5.034	-13	-9.5	-27.6	36.9	-13.3
4.98	6.826	-7.6	-4.2	-11	13.2	-9.6
5.65	6.84	-7.8	-4.2	-10.8	12.7	-10.2
Interaction 4 (Form I and Form I')						
0	8.073	-9.2	-3.3	-9.7	8.6	-13.6
1.58	7.71	-18.5	-7.8	-15.7	28.7	-13.3
1.9	7.739	-17.5	-7.8	-15.3	26.5	-14.1
2.4	7.658	-19.6	-8.3	-16.5	32.5	-11.8
3.23	7.603	-20.6	-9.3	-17.6	35.8	-11.7
3.46	7.576	-21.8	-10	-18	38.1	-11.6
3.99	7.538	-23	-10.3	-18.8	40.7	-11.5
4	7.533	-23.1	-10.4	-18.9	41.1	-11.3
4.33	7.494	-24.3	-10.8	-19.6	44.3	-10.4
4.98	7.839	-13.2	-5.4	-14	19.6	-13.1
5.65	7.847	-13.2	-5.4	-14.2	19.3	-13.5
Interaction 5 (Form I and Form I')						
0	7.348	-9.6	-4.1	-11.8	12.9	-12.6
1.58	7.261	-12.1	-5.8	-13.6	20	-11.5
1.9	7.268	-11.4	-5.4	-13.5	18.7	-11.6
2.4	7.248	-12.6	-6.2	-13.9	21.6	-11.3
3.23	7.236	-13.2	-6.7	-14.4	23.4	-10.9
3.46	7.224	-13.6	-7	-14.7	24.6	-10.7
3.99	7.224	-13.7	-7.1	-14.8	25.2	-10.4
4	7.218	-13.8	-7.2	-14.9	25.6	-10.3
4.33	7.206	-14.3	-7.5	-15.2	27.1	-9.9
4.98	7.809	-13.2	-5.8	-11.1	19	-11.2
5.65	7.829	-12.7	-5.5	-10.5	17.7	-11.1
Interaction 6 (Form I and Form I')						

0	5.754	-3.8	-2	-14.2	7.2	-12.9
1.58	5.698	-6.8	-3.3	-19.3	16.1	-13.4
1.9	5.712	-6.3	-3.1	-18.4	14.6	-13.2
2.4	5.679	-7.8	-4	-20.4	18.6	-13.6
3.23	5.682	-9.2	-5.1	-22	22.8	-13.6
3.46	5.679	-9.8	-5.5	-22.7	24.7	-13.4
3.99	5.677	-11	-5.9	-23.7	27.5	-13.2
4	5.674	-11.2	-6	-23.9	28	-13.1
4.33	5.668	-12.3	-6.4	-24.8	31	-12.5
4.98	3.41	-13.6	-10.3	-52.2	83.1	6.9
5.65	3.408	-13.6	-10.4	-52.1	83.4	7.3
Interaction 7 (Form I)						
0	5.179	0	-1.5	-17.8	9.1	-10.2
1.58	4.802	-4	-2.8	-25	21.1	-10.7
1.9	4.821	-3.9	-2.9	-24.8	20.2	-11.3
2.4	4.76	-5	-3.2	-26	23.2	-11
3.23	4.689	-6.6	-3.8	-28.1	27.2	-11.3
3.46	4.654	-7.2	-4.1	-29.1	29.5	-10.9
3.99	4.616	-7.8	-4.4	-30.1	31.8	-10.4
4	4.615	-7.9	-4.4	-30.1	31.9	-10.5
4.33	4.573	-9.2	-4.8	-31.2	34.7	-10.5
Interaction 8 (Form I')						
4.98	3.41	-13.6	-10.3	-52.2	83.1	6.9
5.65	3.408	-13.6	-10.4	-52.1	83.4	7.3

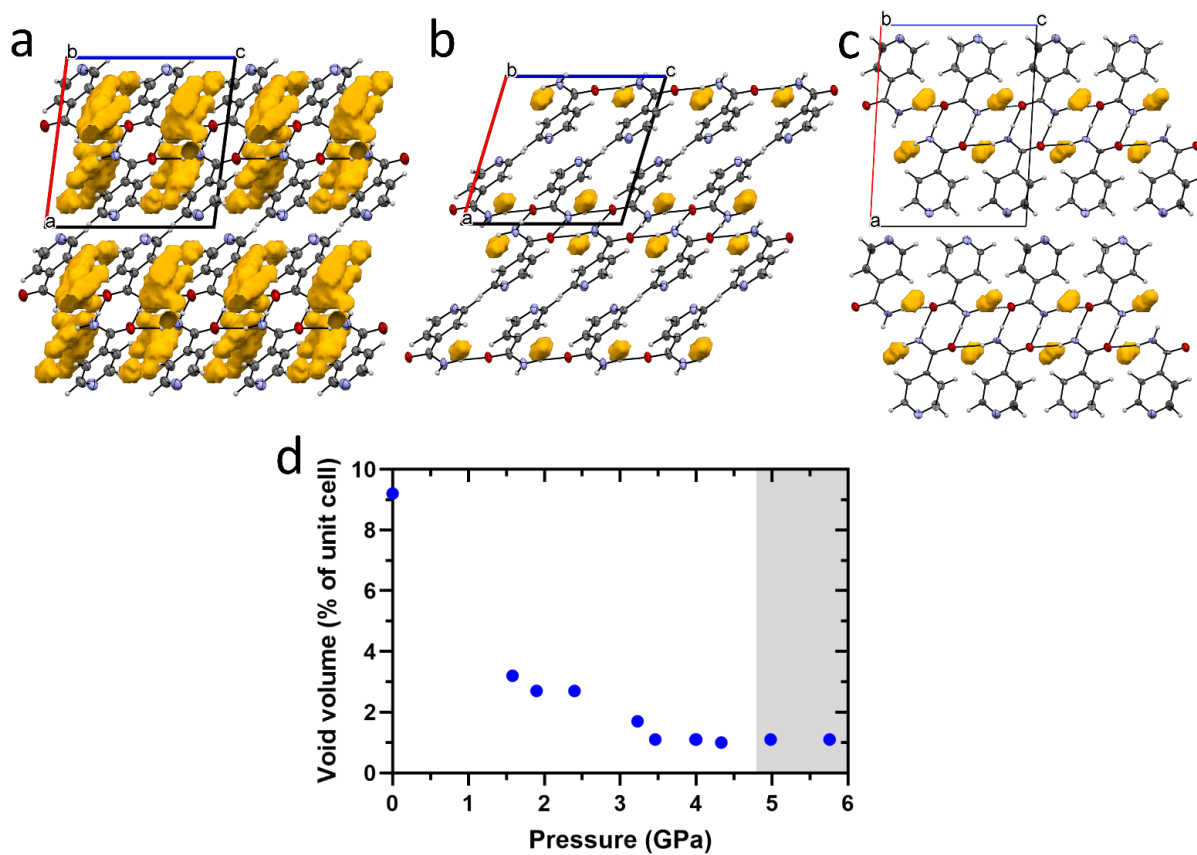


**Fig. S8.** Void analysis of isonicotinamide Form I with a probe radius of 0.5 Å and approximate grid spacing of 0.2 Å at a) ambient pressure; b) 4.33 GPa and c) Form I' at 4.98 GPa. All structures are viewed down the b-axis. d) Void volume of isonicotinamide Form I and Form I' (highlighted in grey).

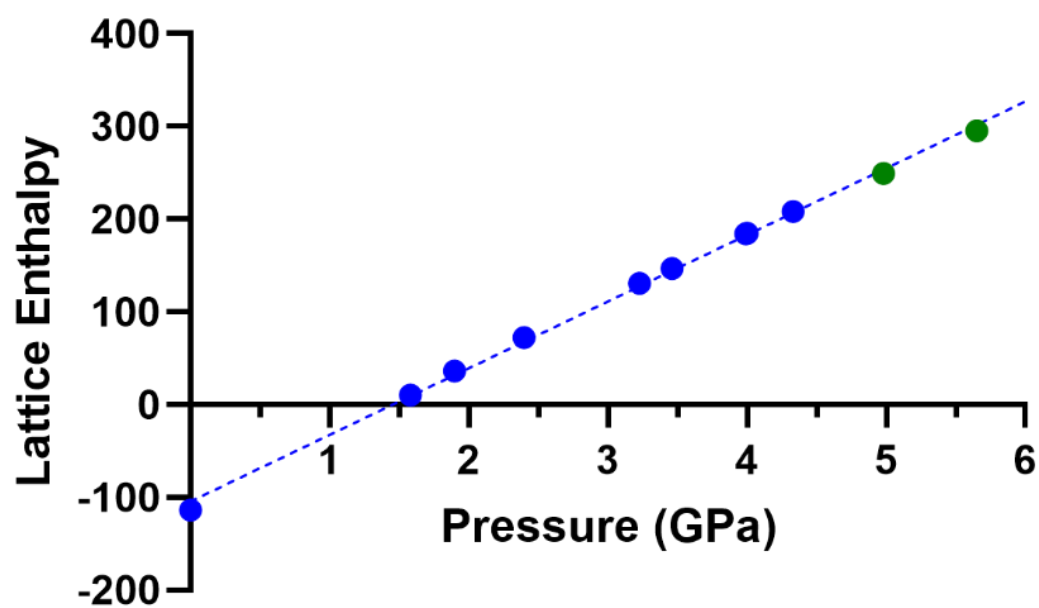


**Fig. S9.** Enthalpy of Form I isonicotinamide and Form I' are shown in blue and green respectively, as a function of pressure. Enthalpy values ( $H$ ) are calculated by  $H = U + PV$ , where  $U$  is the internal energy ( $\text{kJ mol}^{-1}$ ),  $P$  is pressure (Pa) and  $V$  is the volume ( $\text{m}^3$ ).

## REFERENCES

- 1 N. Tateiwa and Y. Haga, *Rev. Sci. Instrum.*, 2009, **80**, 123901.
- 2 G. J. Piermarini, S. Block, J. D. Barnett and R. A. Forman, *J. Appl. Phys.*, 1975, **46**, 2774–2780.
- 3 Bruker AXS Inc., 2017.
- 4 Bruker AXS Inc., 2018.
- 5 G. M. Sheldrick, 2008.
- 6 O. V. Dolomanov, L. J. Bourhis, R. J. Gildea, J. A. K. Howard and H. Puschmann, *J. Appl. Crystallogr.*, 2009, **42**, 339–341.
- 7 C. B. Aakeröy, A. M. Beatty, B. A. Helfrich and M. Nieuwenhuyzen, *Cryst. Growth Des.*, 2003, **3**, 159–165.
- 8 C. R. Groom, I. J. Bruno, M. P. Lightfoot and S. C. Ward, *Acta Crystallogr. Sect. B*, 2016, **72**, 171–179.
- 9 B. Delley, *J. Chem. Phys.*, 1990, **92**, 508–517.
- 10 Accelrys Software, 2011.
- 11 J. P. Perdew, J. A. Chevary, S. H. Vosko, K. A. Jackson, M. R. Pederson, D. J. Singh and C. Fiolhais, *Phys. Rev. B*, 1992, **46**, 6671–6687.
- 12 A. Tkatchenko and M. Scheffler, *Phys. Rev. Lett.*, 2009, **102**, 73005.
- 13 H. J. Monkhorst and J. D. Pack, *Phys. Rev. B*, 1976, **13**, 5188–5192.
- 14 M. G. Reeves, P. A. Wood and S. Parsons, *J. Appl. Crystallogr.*, 2020, **53**, 1154–1162.
- 15 M. J. Frisch, G. W. Trucks, H. B. Schlegel, G. E. Scuseria, M. A. Robb, J. R. Cheeseman, G. Scalmani, V. Barone, B. Mennucci, G. A. Petersson, H. Nakatsuji, M. Caricato, X. Li, H. P. Hratchian, A. F. Izmaylov, J. Bloino, G. Zheng, J. L. Sonnenberg, M. Hada, M. Ehara, K. Toyota, R. Fukuda, J. Hasegawa, M. Ishida, T. Nakajima, Y. Honda, O. Kitao, H. Nakai, T. Vreven, J. A. Montgomery, J. E. Peralta, F. Ogliaro, M. Bearpark, J. J. Heyd, E. Brothers, K. N. Kudin, V. N. Staroverov, R. Kobayashi, J. Normand, K. Raghavachari, A. Rendell, J. C. Burant, S. S. Iyengar, J. Tomasi, M. Cossi, N. Rega, J. M. Millam, M. Klene, J. E. Knox, J. B. Cross, V. Bakken, C. Adamo, J. Jaramillo, R. Gomperts, R. E. Stratmann, O. Yazyev, A. J. Austin, R. Cammi, C. Pomelli, J. W. Ochterski, R. L. Martin, K. Morokuma, V. G. Zakrzewski, G. A. Voth, P. Salvador, J. J. Dannenberg, S. Dapprich, A. D. Daniels, J. B. Farkas; Foresman, J. V. Ortiz, J. Cioslowski and D. J. Fox, 2009.
- 16 C. F. Macrae, I. Sovago, S. J. Cottrell, P. T. A. Galek, P. McCabe, E. Pidcock, M. Platings, G. P. Shields, J. S. Stevens, M. Towler and P. A. Wood, *J. Appl. Crystallogr.*, 2020, **53**, 226–235.
- 17 M. Bakiler, O. Bolukbasi and A. Yilmaz, *J. Mol. Struct.*, 2007, **826**, 6–16.
- 18 J. L. Castro, J. F. Arenas, M. R. Lopez-Ramirez, J. Soto and J. C. Otero, *J. Colloid Interface Sci.*, 2013, **396**, 95–100.
- 19 G. M. Sheldrick, *Acta Crystallogr. Sect. A Found. Crystallogr.*, 2015, **71**, 3–8.

- 20 G. M. Sheldrick, *Acta Crystallogr. Sect. C Struct. Chem.*, 2015, **71**, 3–8.
- 21 M. J. Cliffe and A. L. Goodwin, *J. Appl. Crystallogr.*, 2012, **45**, 1321–1329.